PV Hosting Capacity Assessment of Storage-Integrated Distribution Systems with Constrained PV Curtailment and Load Shedding under Fault Conditions

Yi Wang, *Member*, *IEEE*, Yuxuan Huang, Shida Zhang, *Member*, *IEEE*, Aiwen Jiang, *Member*, *IEEE*, Yaoqiang Wang, *Senior Member*, *IEEE*, Venkata Dinavahi, *Fellow*, *IEEE*, and Jun Liang, *Fellow*, *IEEE*

***Abstract*—In recent years, distributed photovoltaic (PV) systems have experienced accelerated deployment in distribution networks, driven by inherent advantages. However, high-penetration PV integration introduces critical operational challenges, including voltage violations and reverse power flows, which become progressively more pronounced as penetration levels increase and may ultimately harm user interests. To comprehensively assess the network's PV hosting capacity (PVHC) while safeguarding the interests of both PV owners and load consumers, this paper proposes a novel stochastic bi-scenario (pre-fault and post-fault) assessment framework which explicitly quantifies and constrains post-fault PV curtailment and load shedding, mediated by battery energy storage (ES) systems. We derive an analytical linearized expression for the nonlinear PV curtailment under all N-1 contingencies, transforming the original PVHC assessment model into a tractable mixed-integer linear programming (MILP) model. Furthermore, our analysis reveals that, an inherent trade-off exists between reducing fault-induced PV curtailment and enhancing load reliability in storage-integrated grids due to state of charge (SOC) constraints, which holds significant guiding importance for the practical industrial application of PV integration. Finally, the effectiveness, and scalability of the proposed method are verified through different test systems.**

***Index Terms*—Distribution networks, PV hosting capacity, Post-fault analysis, PV curtailment, Reliability constraints.**

This work was supported in part by the Natural Science Foundation of Henan under Grant 242300421167, in part by the National Natural Science Foundation of China under Grant 62203395, in part by the Project of Young Talent Promotion of Henan Association for Science and Technology under Grant 2025HYTP028, in part by the China Postdoctoral Science Foundation under Grant 2023TQ0306, and in part by the Postdoctoral Research Project of Henan Province under Grant 202101011. (*Corresponding author: Shida Zhang*)

Yi Wang, Yuxuan Huang, Shida Zhang, Yaoqiang Wang are with the School of Electrical and Information Engineering, Zhengzhou University, Zhengzhou 450001, China (e-mails:wangyi1414599008@163.com; 13569634790@163.com; zhangshida@zzu.edu.cn; wangyqee@163.com).

Aiwen Jiang is with the School of Artificial Intelligence, Jiangxi Normal University, Nanchang 330022, China (e-mail:jiangaiwen@jxnu.edu.cn).

Venkata Dinavahi is with the Department of Electrical and Computer Engineering, University of Alberta, Edmonton, AB T6G 2V4, Canada (e-mail: dinavahi@ualberta.ca).

Jun Liang is with the School of Engineering, Cardiff University, Cardiff CF24 3AA, U.K. (e-mail: liangj1@cardiff.ac.uk).

I. Introduction

Distributed PV systems, leveraging core merits including flexible deployment, low-carbon footprint, high energy efficiency, and sustainable utilization, have emerged as a pivotal catalyst driving the global energy transition. However, compared to conventional power generation sources, PV systems exhibit pronounced temporal discrepancies with load profiles (i.e., Source-load profile mismatch [1]) and uncertainty. This characteristic may cause multiple operational risks in distribution systems with high penetration of PV [2], [3], such as overvoltage and overcurrent violations [4]. Furthermore, during fault scenarios, this high level of penetration significantly amplifies these potential safety risks. To guide users to orderly configure PV and avoid these problems, it is necessary to accurately assess the capacity of PV known as the PVHC. However, conducting a comprehensive PVHC assessment that considers both normal and fault operating scenarios presents significant challenges due to its inherent complexity.

In the existing literature, several methods have been proposed for evaluating the hosting capacity of PV power in distribution networks. Reference [5] systematically summarizes the quantitative methods (deterministic methods, probabilistic methods, optimization-driven methods, data-driven methods) for the PVHC, and compares their technical principles, applicable scenarios, and limitations; Reference [6] evaluated the PVHC of distribution networks by incrementally increasing PV penetration, verifying voltage and thermal stability limits, and applying system reconfiguration to raise the capacity upper limit. Reference [7] presents a fuzzy-possibilistic method that integrates α-Cut sets and Monte Carlo simulation to evaluate PVHC through interval modeling of PV variability, without requiring probability distributions. Reference [8] uses a hybrid stochastic method, combining Monte Carlo simulation and 90% planning risk quantile, to evaluate the PVHC of distribution networks under overvoltage and overload constraints. Reference [9] proposes a general method based on nomogram representation for evaluating the PVHC affected by over-voltage curtailment. Reference [10] constructs a feasible region model for PV access capacity at multiple potential access locations, representing the constraints of the maximum access capacity of PV power among different locations. However, most of the above-mentioned studies mainly focus on the PV capacity limit under

voltage and power constraints during normal operation, without considering the situation after any fault.

Adjusting PV output during contingencies is a common operational response [11]-[13]. However, PVHC assessment based on direct curtailment strategies may yield overestimated results, and the curtailed energy may be unreasonably amplified, thereby harming the interests of PV owners [35]. Conversely, completely prohibiting curtailment leads to overly conservative assessment due to the impracticality of perfect post-fault generation-load matching. Therefore, permitting constrained PV curtailment, with reasonable limits, is essential for realistic PVHC evaluation. Reference [33] instructs inverters to reduce PV active power to a specific value post-fault via commands from the dispatch center, yet it lacks a concrete curtailment scheme.

Common approaches include setting maximum curtailment limits or maximum curtailment proportions. Literature [14] focuses on PVHC assessment under both normal operating conditions and high-impact fault scenarios, limiting PV curtailment to within 7%. However, this simple and mandatory curtailment ratio setting may lead to unreasonable curtailment schemes, as alternatives potentially exist that could achieve a lower total curtailment (or a smaller economic value loss). In practice, users are typically more concerned with their tolerance for the overall loss, rather than the loss proportion of individual PV units. However, due to characteristics such as nonlinearity and the difficulty of deriving an analytical expression for total curtailment, no studies have yet incorporated it as a constraint in PVHC assessment model. Notably, analytical methods for quantifying post-fault load losses (from reliability assessment theory) are well-established [15]-[18] providing critical references for curtailment loss quantification.

Notably, ES, as core regulating resources in renewable-integrated distribution networks, enhances operational efficiency through peak shaving and valley filling [19], regulates voltage, and improves PVHC during normal operation [20]. Under contingency scenarios, ES demonstrates significant value in two key aspects: on one hand, by discharging, it provides active power support to promote power supply restoration and enhance system reliability [21]-[24], as exemplified by existing studies [25] that integrate ES with network reconfiguration to minimize outage losses during faults; on the other hand, through charging, it absorbs

Nomenclature

General Notation in Two Scenarios

Variables

$P_{i,t}^{\mathrm{PV}}$	The PV output power
$P_{i,t}^{\mathrm{load}}$, $Q_{i,t}^{\mathrm{load}}$	Active loads and reactive loads of bus *i*

Parameters

r_{ij} , x_{ij}	Resistance and reactance of branch *ij*
$V_{\min}$, $V_{\max}$	Limitation of bus voltage
$P_{ij,\min}$, $P_{ij,\max}$	Limitation of branch active power
$Q_{ij,\min}$, $Q_{ij,\max}$	Limitation of branch reactive power
$P_{\min}^{\mathrm{ess}}$, $P_{\max}^{\mathrm{ess}}$	Limitation of charging-discharging power
$SOC_{\min}$, $SOC_{\max}$	Limitation of SOC

Sets

Ω_{L}	The set of branches
Ω_{N}	The set of buses
Ω_{time}	The set of all time intervals in a typical day
N_{b}	Number of buses

Notation in Pre-Fault Scenario

Variables

$P_{i,t}^{\mathrm{ess}}$	Charging and discharging power of the ES
$P_{ij,t}$, $Q_{ij,t}$	Active power and reactive power of branch *ij*
$V_{i,t}$	The square of the voltage at bus *i*
$SOC_{i,t}$	The SOC of the storage unit
$Pg_{i,t}$, $Qg_{i,t}$	Active and reactive power injected by the substation
$P_{i,t}^{\mathrm{in}}$, $Q_{i,t}^{\mathrm{in}}$	Active power and reactive power of bus injection

Binary Variables

$s_{ij,t}$	1 when branch *ij* is connected

Notation in Post-Fault Scenario

Variables

$P_{i,t}^{\mathrm{in},xy}$, $Q_{i,t}^{\mathrm{in},xy}$	Active power and reactive power of bus injection under a fault on branch *xy*
$Pg_{i,t}^{xy}$ $Qg_{i,t}^{xy}$	Active and reactive power injected by the substation under a fault on branch *xy*
$P_{ij,t}^{xy}$, $Q_{ij,t}^{xy}$	Active power and reactive power of branch *ij* under a fault on branch *xy*
$P_{i,t}^{\mathrm{ess},xy}$	Charging and discharging power of the ES under a fault on branch *xy*
$L_{i,t}^{xy}$	The curtailment coefficient
$P_{i,t}^{\mathrm{curt},xy}$	The curtailed PV power
$V_{i,t}^{xy}$	The square of the voltage at bus *i* under a fault on branch *xy*

Parameters

λ^{xy}	Outage rate of the branch *xy*
$G^{\exp}$	The limitation of PV curtailment
$H^{\exp}$	The limitation of the reliability index

Binary Variables

$p_{i,t}^{xy}$	Indicator of whether bus *i* is affected due to a fault in the branch connecting buses *x* and *y*.
$q_{i,t}^{xy}$	1 when the demand of bus *i* is completely recovered due to a fault in branch *xy*
$y_{i,t,s}$	Adaptive McCormick partitioning variable
$s_{ij,t}^{xy}$	1 when branch *ij* is connected after network reconfiguration due to a fault in branch *xy*

Sets

Ω_{F}	The set of N-1 contingencies

otherwise curtailed PV generation, protecting PV owners' interests while ensuring technical effectiveness and economic rationality in PVHC assessment.

However, a not yet fully clarified conflict exists in the application of ES for simultaneously ensuring power supply reliability and minimizing PV curtailment during grid faults. Under ES support, a complex, coupled, and constraining relationship exists among PVHC, expected power supply reliability, and PV curtailment during faults. There is an urgent need for ES-integrated PVHC methodologies that safeguard the interests of both load consumers and PV owners.

To fill the knowledge gap in the aforementioned studies, in this paper, we propose a PVHC assessment method in storage-integrated distribution systems, considering post-fault PV curtailment and load shedding constraints. The main contributions of this work can be summarized as follows.

1) To quantify the losses that PV owners may incur under potential distribution-network faults, we derive an analytical expression for the expected PV curtailment, explicitly considering both post-fault network reconfiguration and battery-energy-storage support. This analytical metric provides the quantitative basis for safeguarding PV owners' interests.

2) By embedding the PV curtailment and load shedding constraints, a stochastic bi-scenario (pre-fault and post-fault) PVHC assessment framework is proposed. The application of this method can simultaneously protect the interests of PV owners and load consumers.

3) Based on the proposed method, we uncover the inherent trade-off between reducing fault-induced PV curtailment and enhancing load reliability with PVHC held constant. Further analysis finds that this is due to the competition between these two factors for the utilization of the limited SOC in ES applications, which holds significant guiding importance for the practical industrial application of PV integration.

The rest of the paper is organized as follows. Section II presents the model's objective function, system security constraints under both pre-fault and post-fault conditions, and the overall framework of the paper. Section III provides a detailed exposition of the pre-fault model. Section IV provides a detailed exposition of the post-fault model. Section V provides a detailed PV curtailment constraint and reliability constraint. Section VI validates the effectiveness and scalability of the proposed model and evaluation methodology with both the 10-bus and IEEE 33-bus systems. Section VII provides a summary and concluding remarks.

II. Problem Description

This section presents the objective function for the PVHC assessment based on a bi-scenario framework which considers system security constraints under both pre-fault and post-fault conditions, along with the reliability constraints and PV curtailment constraints proposed to safeguard user interests.

A. Objective Function

The objective of the proposed framework is to maximize the PVHC under the bi -scenario (pre-fault and post-fault) coupled constraints.

$$\max \ \mathbf{e}^{\mathrm{T}}\mathbf{S}^{\mathrm{PV}}, \tag{1}$$

where $\mathbf{S}^{\mathrm{PV}}=(S_1^{\mathrm{PV}},...,S_i^{\mathrm{PV}},...,S_N^{\mathrm{PV}})^{\mathrm{T}}$ denotes the installed capacity of PV power generation at each location. $\mathbf{e}=(1,\ ...,\ 1)_{N\times 1}$ denotes N-dimensional Unit column vector.

B. Pre-fault system security constraints

Under the pre-fault operation, the state variables of ES and network topology (NT) constitute determinants of PVHC, which are derived from the power flow equations as well as the voltage and power security constraints:

$$\mathbf{F}_t^{\mathrm{pre}}(\mathbf{X}_t^{\mathrm{pre}},\mathbf{Y}_t^{\mathrm{pre}},\mathbf{S}^{\mathrm{PV}})\le\mathbf{0},\quad \forall t\in\Omega_{\mathrm{time}}, \tag{2}$$

where $\mathbf{X}_t^{\mathrm{pre}}$ represents the state variables related to ES in the pre-fault state at time t. $\mathbf{Y}_t^{\mathrm{pre}}$ represents the state variables associated with NT in the pre-fault state. Here the subscript "t" denotes time t. Ω_{time} represents the set of all time intervals in a typical day. Eq. (2) represents the constraint relationship imposed by these two types of state variables on $\mathbf{S}^{\mathrm{PV}}$.

C. Post-Fault System Security Constraints

The proposed PVHC assessment framework takes into account the potential contingency scenarios that may occur at any time in a typical day, specifically the set of all N-1 contingency scenarios is denoted as F= {1, ..., K}. Under the post-fault scenario, the operation of an ES unit evolves from its pre-fault SOC. Therefore, the pre/post-fault state variables of ES and NT influence PVHC, which are derived from the operation security constraints of each post-fault system.

$$\mathbf{F}_t^{\mathrm{post}}(\mathbf{X}_t^{\mathrm{pre}},\mathbf{X}_t^{\mathrm{post}},\mathbf{Y}_t^{\mathrm{pre}},\mathbf{Y}_t^{\mathrm{post}},\mathbf{S}^{\mathrm{PV}})\le\mathbf{0},\ \forall t\in\Omega_{\mathrm{time}} \tag{3}$$

where $\mathbf{X}_t^{\mathrm{post}}=(X_{1,t}^{\mathrm{post}},...,X_{k,t}^{\mathrm{post}},...,X_{K,t}^{\mathrm{post}})$, $\mathbf{Y}_t^{\mathrm{post}}=(Y_{1,t}^{\mathrm{post}},...,Y_{k,t}^{\mathrm{post}},...,Y_{K,t}^{\mathrm{post}})$ represents the state variables related to ES and NT in all fault scenarios k at time t, respectively. Eq. (3) represents the constraints on $\mathbf{S}^{\mathrm{PV}}$ imposed by $\mathbf{X}_t^{\mathrm{pre}}$, $\mathbf{Y}_t^{\mathrm{pre}}$, $\mathbf{X}_t^{\mathrm{post}}$, and $\mathbf{Y}_t^{\mathrm{post}}$ due to the post-fault network security constraints.

D. PV Curtailment Constraint and Reliability Constraint

To safeguard user interests, it is necessary to incorporate both PV curtailment and reliability constraints into the PVHC assessment framework, thereby enabling the analysis of their impacts.

The pre-fault and post-fault variables $(\mathbf{X}_t^{\mathrm{pre}},\mathbf{X}_t^{\mathrm{post}},\mathbf{Y}_t^{\mathrm{pre}},\mathbf{Y}_t^{\mathrm{post}})$ affect the total PV curtailment and load-shedding in all fault scenarios during time interval t. These totals are denoted respectively as $G_t^{\mathrm{post}}(\cdot)$ and $H_t^{\mathrm{post}}(\cdot)$, respectively. Based on this, the two constraints are expressed as follows.

$$\sum_{t=1}^{T}G_t^{\mathrm{post}}(\mathbf{X}_t^{\mathrm{pre}},\mathbf{X}_t^{\mathrm{post}},\mathbf{Y}_t^{\mathrm{pre}},\mathbf{Y}_t^{\mathrm{post}})\le G^{\mathrm{exp}}, \tag{4}$$

$$\sum_{t=1}^{T}H_t^{\mathrm{post}}(\mathbf{X}_t^{\mathrm{pre}},\mathbf{X}_t^{\mathrm{post}},\mathbf{Y}_t^{\mathrm{pre}},\mathbf{Y}_t^{\mathrm{post}})\le H^{\mathrm{exp}}, \tag{5}$$

where G^{exp} denotes the limit for PV curtailment aimed at safeguarding PV owners, and H^{exp} denotes the limit for the reliability index aimed at safeguarding load users

E. Overall Framework of This Paper

The procedural workflow of the proposed methodology, as summarized in Fig. 1. It contains both pre-fault and post-fault scenarios, delineating the three aspects of requirements in the PVHC assessment.

(i) Pre-fault operational security constraints (considering network reconfiguration and multi-timescale regulation of ES);

(ii) Secure operation constraints under N-1 post-fault scenarios (incorporating post-fault network reconfiguration and emergency support from ES);

(iii) For the requirements of safeguarding user interests, including constrained power supply reliability for load consumers and PV curtailment constraints for PV owners.

In the pre-fault operation, distribution networks with ES generate variables of ES and NT, which directly influence the system's PVHC. In fault analysis, these variables are passed to each N-1 contingency scenario, generating corresponding post-fault ES and NT variables for each scenario. Furthermore, PV curtailment and load shedding can be quantified based on ES and NT across all N-1 contingency scenarios. In this paper, due to protection the interest of PV owner and load consumers, both must be constrained. This directly affects the post-fault ES, which indirectly influences the pre-fault ES strategy, thereby impacting the PVHC. Through this closed-loop coupling mechanism, a comprehensive assessment of the PVHC is achieved. Pre-fault operation is detailed in Section III, while post-fault operation is analyzed in Section IV.

III. Pre- Fault Secure Operation Model

Following the (2) stablished in Section II, this section elaborates on the operational constraints required to ensure pre-fault system secure operation. The pre-fault secure operation is characterized by the Constraints (6)-(17).

A. Pre-Fault Power Injection

The pre-fault power flow balance constraints are given by (8)-(9), where the active and reactive power injection at bus i is defined by (6) and (7), respectively.

$$P_{i,t}^{\text{in}} = \sum_{j\in a(i)} P_{ij,t} - \sum_{k\in b(i)} P_{ik,t},\ \forall i \in \Omega_{\text{N}}, ij,\ ik \in \Omega_{\text{L}},\ t \in \Omega_{\text{time}}, \quad (6)$$

$$Q_{i,t}^{\text{in}} = \sum_{j\in a(i)} Q_{ij,t} - \sum_{k\in b(i)} Q_{ik,t},\ \forall i \in \Omega_{\text{N}}, ij,\ ik \in \Omega_{\text{L}},\ t \in \Omega_{\text{time}}, \quad (7)$$

$$P_{i,t}^{\text{in}} + P_{i,t}^{\text{load}} + P_{i,t}^{\text{ess}} - Pg_{i,t} - P_{i,t}^{\text{PV}} = 0,\ \forall i \in \Omega_{\text{N}},\ t \in \Omega_{\text{time}}, \quad (8)$$

$$Q_{i,t}^{\text{in}} + Q_{i,t}^{\text{load}} - Qg_{i,t} = 0,\ \forall i \in \Omega_{\text{N}},\ t \in \Omega_{\text{e}}, \quad (9)$$

where $a(i)$ represents the set of all buses connected to and downstream of the bus i. $b(i)$ represents the set of all buses connected to and upstream of the bus i. Ω_{N} represents the set of buses. $P_{i,t}^{\text{in}}$ and $Q_{i,t}^{\text{in}}$ represent the active and reactive power injected by bus i in the pre-fault state, respectively. $P_{i,t}^{\text{load}}$ and $Q_{i,t}^{\text{load}}$ represent the active and reactive loads of bus i respectively. $P_{i,t}^{\text{ess}}$ represents the charging and discharging power of the ES at bus i (positive value indicates charging, negative value indicates discharging). $Pg_{i,t}$ and $Qg_{i,t}$ represent the active and reactive power injected by the substation at bus i. $P_{i,t}^{\text{PV}}$ represents the PV output at bus i. Ω_{L} denotes the set of branches.

B. Pre-Fault Voltage and Branch Capacity Constraints

Voltage constitutes a critical power quality parameter in distribution networks [26]. As an operational security constraint, it should not exceed its upper and lower limits to guarantee the power quality. In this work, we employ a linear power flow model [27] to formulate network reconfiguration as follows.

$$\begin{cases}(s_{ij,t}-1)+P_{ij,t}r_{ij}+Q_{ij,t}x_{ij} \le V_{i,t}-V_{j,t} \\ (1-s_{ij,t})+P_{ij,t}r_{ij}+Q_{ij,t}x_{ij} \ge V_{i,t}-V_{j,t}\end{cases},\ \forall i,j \in \Omega_{\text{N}},\ ij \in \Omega_{\text{L}},\ t \in \Omega_{\text{time}}, \quad (10)$$

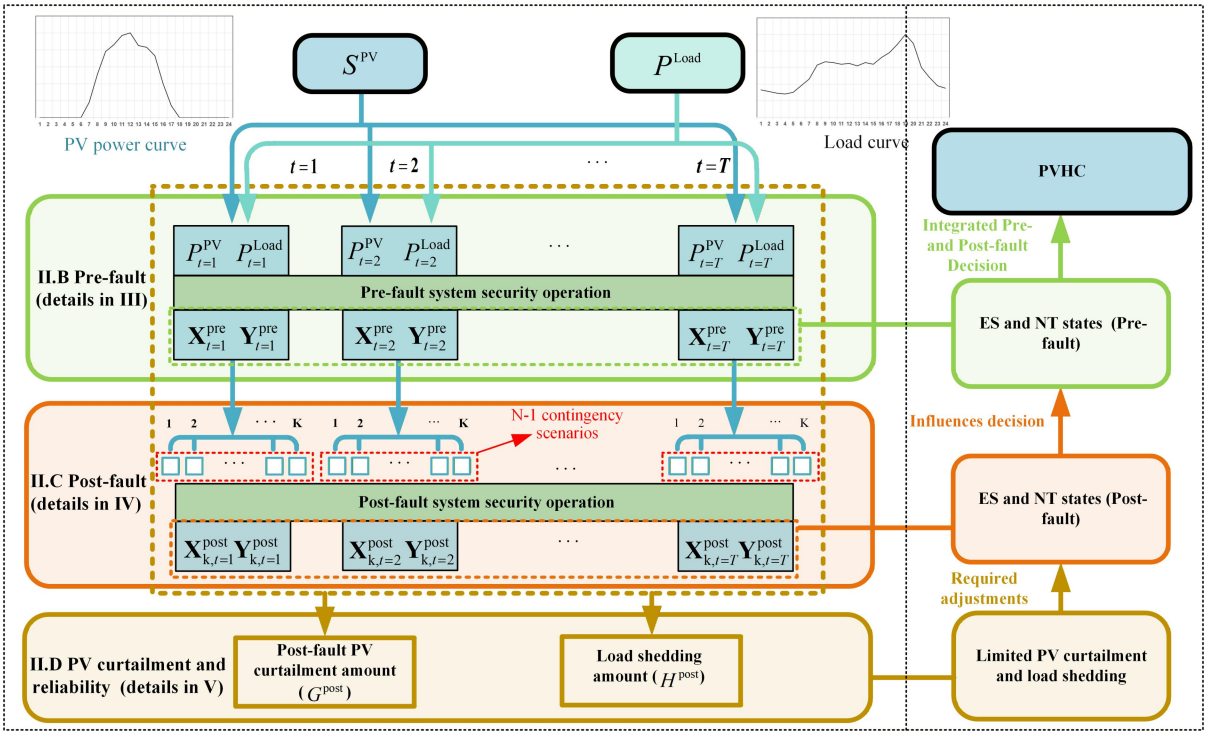

Fig. 1. Transition between pre-fault and post-fault and procedural workflow of the proposed methodology.

$$V_{\min} \le V_{i,t} \le V_{\max},\ \forall i \in \Omega_{\mathrm{N}},\ t \in \Omega_{\mathrm{time}}, \tag{11}$$

$$P_{ij,\min} \le P_{ij,t} \le P_{ij,\max},\ \forall ij \in \Omega_{\mathrm{L}},\ t \in \Omega_{\mathrm{time}}, \tag{12}$$

$$Q_{ij,\min} \le Q_{ij,t} \le Q_{ij,\max},\ \forall ij \in \Omega_{\mathrm{L}},\ t \in \Omega_{\mathrm{time}}, \tag{13}$$

$$\sum_{ij \in \Omega_{\mathrm{L}}} s_{ij,t} = N_{\mathrm{b}} - 1,\ \forall t \in \Omega_{\mathrm{time}}, \tag{14}$$

where $s_{ij,t}$ denotes the switching status of branch *ij* in the pre-fault state ($s_{ij,t}=1$ indicates the branch is closed, while $s_{ij,t}=0$ is open). $V_{i,t}$ represents the square of the voltage at bus *i*. $V_{\max}$ and $V_{\min}$ are the upper bound and lower bound for the square of the voltage amplitude. $P_{ij,t}$ and $Q_{ij,t}$ are the active power and reactive power flowing from bus *i* to bus *j*. $P_{ij,\max}$ and $P_{ij,\min}$ are the upper bound and lower bound of active power for the branches. $Q_{ij,\max}$ and $Q_{ij,\min}$ are the upper bound and lower bound of reactive power for the branches. r_{ij} and x_{ij} are the resistance and reactance of branch *ij*, respectively. N_{b} represents the number of buses, (14) denotes the radial constraint to ensure unidirectional power flow.

C. Pre-Fault ES Operation Constraints

In ES unit constraints, the permissible charging/ discharging limits of power are expressed in (15), the SOC limits in (17).

$$P_{\min}^{\mathrm{ess}} \le P_{i,t}^{\mathrm{ess}} \le P_{\max}^{\mathrm{ess}},\ \forall i \in \Omega_{\mathrm{N}},\ t \in \Omega_{\mathrm{time}}, \tag{15}$$

$$\begin{cases} P_{i,t}^{\mathrm{C,loss}} = (1-\eta^{C})P_{i,t}^{\mathrm{ess}} \\ P_{i,t}^{\mathrm{D,loss}} = (1-\dfrac{1}{\eta^{D}})P_{i,t}^{\mathrm{ess}} \\ P_{i,t}^{\mathrm{loss}} = \max(P_{i,t}^{\mathrm{C,loss}}, P_{i,t}^{\mathrm{D,loss}}) \end{cases},\ \forall i \in \Omega_{\mathrm{N}},\ t \in \Omega_{\mathrm{time}}, \tag{16}$$

$$\begin{cases} SOC_{i,t} = SOC_{i,t-1} + P_{i,t}^{\mathrm{ess}} - P_{i,t}^{\mathrm{loss}} \\ SOC_{\min} \le SOC_{i,t} \le SOC_{\max} \end{cases},\ \forall i \in \Omega_{\mathrm{N}},\ t \in \Omega_{\mathrm{time}}, \tag{17}$$

where $P_{\max}^{\mathrm{ess}}$ and $P_{\min}^{\mathrm{ess}}$ are the upper and lower bounds of the charging-discharging power, respectively; $SOC_{i,t}$ denotes the SOC of the storage unit at bus *i* in the pre-fault state. $P_{i,t}^{\mathrm{C,loss}}$ and $P_{i,t}^{\mathrm{D,loss}}$ are charging and discharging power loss, respectively. $SOC_{\max}$ and $SOC_{\min}$ are the upper bound and lower bound of the SOC. The overcharging or over-discharging of the ES is avoided to prevent damage to its lifespan.

The constraints involved in the pre-fault secure operation model are shown in Fig. 2.

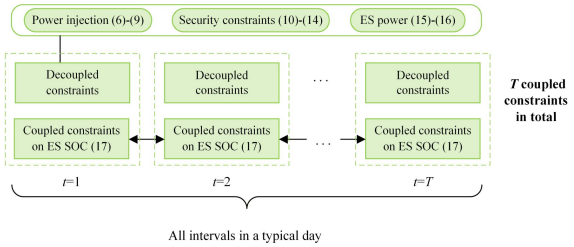

Fig. 2. Pre-fault system security constraints.

D. Impact of PV Uncertainty Considering Correlation and Its Reformulation

The PV power output $P_{i,t}^{\mathrm{PV}}$ at different locations at the same time is uncertain [28], [34], and these uncertainties are correlated, which can be modeled using a normal distribution [29]. The correlation between PV outputs at bus *i* and bus *j*, the PV outputs can be modeled as follows.

$$\begin{cases} \tilde{P}_{i,t}^{\mathrm{PV}} = P_{i,t}^{\mathrm{PV,fcst}} + \Delta P_{i,t}^{\mathrm{PV,error}} \\ \left(\tilde{P}_{i,t}^{\mathrm{PV}}, \tilde{P}_{j,t}^{\mathrm{PV}}\right) \sim \mathcal{N}_{\mathrm{bivariate}}\left(P_{i,t}^{\mathrm{PV,fcst}}, \tilde{P}_{j,t}^{\mathrm{PV,fcst}}, \left(\sigma^{\mathrm{PV}} P_{i,t}^{\mathrm{PV,fcst}}\right)^2, \left(\sigma^{\mathrm{PV}} P_{i,t}^{\mathrm{PV,fcst}}\right)^2, \rho_{ij,t}^{\mathrm{PV}}\right) \end{cases} \tag{18}$$

$$\forall i, j \in \Omega_{\mathrm{N}},\ t \in \Omega_{\mathrm{time}}$$

where σ^{PV} denotes standard deviation coefficients. Coefficient $\rho_{ij,t}^{\mathrm{PV}}$ reveals the correlation between PV outputs at different buses. Rewriting (18) as matrix form, although a single PV unit might follow other distributions, when the PV system comprises numerous and geographically dispersed units, the PV outputs in each period follows the *N*-dimensional multivariate Gaussian distributions in (19) [36], which can be justified by the Central Limit Theorem [37].

$$\tilde{\mathbf{P}}_{t}^{\mathrm{PV}} \sim \mathcal{N}_{\omega}\left(\mathbf{P}_{t}^{\mathrm{PV,fcst}}, \boldsymbol{\Sigma}_{t}^{\mathrm{PV}}\right),\ \forall t \in \Omega_{\mathrm{time}}, \tag{19}$$

where ω is the number of PV units. Under this influence, the power injection $P_{i,t}^{\mathrm{in}}$ becomes a random variable, and the matrix form of the injections (8) is updated as follows.

$$\tilde{\mathbf{P}}_{t}^{\mathrm{in}} + \mathbf{P}_{t}^{\mathrm{load}} + \mathbf{P}_{t}^{\mathrm{ess}} - \mathbf{P}\mathbf{g}_{t} - \tilde{\mathbf{P}}_{t}^{\mathrm{PV}} = 0,\ \forall t \in \Omega_{\mathrm{time}}. \tag{20}$$

The N-dimensional multivariate Gaussian distribution that active power injections follow can be formulated as follows.

$$\tilde{\mathbf{P}}_{t}^{\mathrm{in}} \sim \mathcal{N}_{\omega}\left(\boldsymbol{\mu}_{t}^{\mathrm{P}}, \boldsymbol{\Sigma}_{t}^{\mathrm{P}}\right),\ \forall t \in \Omega_{\mathrm{time}}. \tag{21}$$

Based on the information of related random variables in (19), the expressions of the elements in (21) are shown in (22).

The elements related to active power

$$\begin{cases} \boldsymbol{\mu}_{t}^{\mathrm{P}} = -\mathbf{P}_{t}^{\mathrm{load}} - \mathbf{P}_{t}^{\mathrm{ess}} + \mathbf{P}\mathbf{g}_{t} + \mathbf{P}_{t}^{\mathrm{PV,fcst}} \\ \boldsymbol{\Sigma}_{t}^{\mathrm{P}} = \boldsymbol{\Sigma}_{t}^{\mathrm{PV}} \end{cases},\ \forall t \in \Omega_{\mathrm{time}}. \tag{22}$$

Since state variables have been transformed as random variables, it is necessary to rewrite the security constraints (11)-(12) as chance constraints, which reflect restrictions on the probability of exceeding the limits.

$$\Pr\left\{V_{\min} \le \tilde{V}_{i,t} \le V_{\max}\right\} \ge 1 - p^{\mathrm{V}},\ \forall i \in \Omega_{\mathrm{N}},\ t \in \Omega_{\mathrm{time}}, \tag{23}$$

$$\Pr\left\{P_{ij,\min} \le \tilde{P}_{ij} \le P_{ij,\max}\right\} \ge 1 - p^{\mathrm{S}},\ \forall ij \in \Omega_{\mathrm{L}},\ t \in \Omega_{\mathrm{time}}, \tag{24}$$

where $\Pr\{\bullet\}$ is the probability that inequality constraints hold. Since a linear power flow formulation is adopted in this paper, both voltage $V_{i,t}$ and branch power $P_{ij,t}$ also follow normal distributions under the influence of PV uncertainty. Taking voltage as an example, its distribution can be expressed as follows:

$$\tilde{\mathbf{V}}_{t} \sim \sqrt{\boldsymbol{\Sigma}_{t}^{\mathrm{V}}}\boldsymbol{\Phi} + \boldsymbol{\mu}_{t}^{\mathrm{V}},\ \forall t \in \Omega_{\mathrm{time}}, \tag{25}$$

where $\boldsymbol{\Phi}$ is the vector of standardized normal distributions. $\boldsymbol{\Sigma}_{t}^{\mathrm{V}}$ is the covariance matrix of voltage, $\boldsymbol{\mu}_{t}^{\mathrm{V}}$ is the mean value of voltage. These variables are influenced by the NT s_{ij}, the power of ES, the load, and the installed capacity of PV S^{PV}. Their analytical expressions can be derived based on the aforementioned relationships and will not be elaborated here. Then, the transformations of security constraints (23) are proposed as follows.

The chance constraints (23) can be rewritten as two parts because there is little probability of breaking the constraint from both sides:

$$\begin{cases} \Pr\left\{\tilde{V}_{i,t} \le V_{\max}\right\} \ge 1-p^{\mathrm{V}} \\ \Pr\left\{\tilde{V}_{i,t} \ge V_{\min}\right\} \le p^{\mathrm{V}} \end{cases}, \ \forall i \in \Omega_{\mathrm{N}},\ t \in \Omega_{\mathrm{time}} \quad (26)$$

Based on (25), chance constraints (26) can be transformed as follows:

$$\begin{cases} \mu_{i,t}^{\mathrm{V}} + \Phi^{-1}\left(1-p^{\mathrm{V}}\right)\sqrt{\Sigma_t^{\mathrm{V}}(i,i)} \le V_{\max} \\ \mu_{i,t}^{\mathrm{V}} - \Phi^{-1}\left(p^{\mathrm{V}}\right)\sqrt{\Sigma_t^{\mathrm{V}}(i,i)} \ge V_{\min} \end{cases}, \ \forall i \in \Omega_{\mathrm{N}},\ t \in \Omega_{\mathrm{time}}, (27)$$

where Φ^{-1} is the inverse function of standardized normal distribution. When p^{V} is smaller than 0.5, (27) can be transformed as linear constraints (28) and second-order cone constraints (29).

$$\begin{cases} \Phi^{-1}\left(1-p^{\mathrm{V}}\right)\lambda_{\mathrm{Vmax},i,t} = V_{\max} - \mu_{i,t}^{\mathrm{V}} \\ \Phi^{-1}\left(1-p^{\mathrm{V}}\right)\lambda_{\mathrm{Vmin},i,t} = \mu_{i,t}^{\mathrm{V}} - V_{\min} \end{cases}, \ \forall i \in \Omega_{\mathrm{N}},\ t \in \Omega_{\mathrm{time}}, (28)$$

$$\begin{cases} \lambda_{\mathrm{Vmax},i,t}^2 \ge \Sigma_t^{\mathrm{V}}(i,i) \\ \lambda_{\mathrm{Vmin},i,t}^2 \ge \Sigma_t^{\mathrm{V}}(i,i) \end{cases}, \ \forall i \in \Omega_{\mathrm{N}},\ t \in \Omega_{\mathrm{time}}, \quad (29)$$

where $\lambda_{\mathrm{Vmax},i,t}$, $\lambda_{\mathrm{Vmin},i,t}$ denote auxiliary variables which are greater than or equal to the variance of bus voltage $\Sigma_t^{\mathrm{V}}(i,i)$. $\Sigma_t^{\mathrm{V}}(i,i)$ represents linear combination. Through the aforementioned transformations, the uncertainty model has been converted into a deterministic one. The resulting PVHC assessment model, incorporating the above constraints, is a mixed-integer second-order cone programming model, which can be solved efficiently. The branch power flow constraints (24) are handled in a similar manner and are not presented to conserve space.

It should be noted that the post-fault condition analysis in Section IV is also affected by PV uncertainty. A similar methodology is applied, which involves extensive derivations. We do not present the details as they are not the core contribution of this paper and to conserve space.

IV. Post-Fault Secure Operation Model for Each N-1 Fault

Following the (3) established in Section II, this section elaborates on the operational constraints required to ensure post-fault system secure operation. The post-fault secure operation model of the distribution network is characterized by constraints (30)-(35). The superscript *xy* is used to describe the outage scenario in constraints (30)-(46) due to the fault at branch *xy*, the fault on line *xy* is one of the contingencies in the set Ω_{F}.

The constraints involved in the post-fault secure operation model are shown in Fig. 3.

A. Post-Fault Bus Injection

The power flow balance constraints in the post-fault state are given by (30). To calculate post-fault PV curtailment, we introduce the PV curtailment coefficient $L_{i,t}^{xy}$:

$$\begin{cases} P_{i,t}^{\mathrm{in},xy} + P_{i,t}^{\mathrm{load}} q_{i,t}^{xy} + P_{i,t}^{\mathrm{ess},xy} - Pg_{i,t}^{xy} = L_{i,t}^{xy} P_{i,t}^{\mathrm{PV}} \\ Q_{i,t}^{\mathrm{in},xy} + Q_{i,t}^{\mathrm{load}} q_{i,t}^{xy} = Qg_{i,t}^{xy} \end{cases}, \quad (30)$$
$$\forall i \in \Omega_{\mathrm{N}},\ \Omega_{\mathrm{time}},\ xy \in \Omega_{\mathrm{F}}$$

where $P_{i,t}^{\mathrm{in},xy}$ and $Q_{i,t}^{\mathrm{in},xy}$ denote the active and reactive injection power at bus *i* in the post-fault state, respectively; $Pg_{i,t}^{xy}$ and $Qg_{i,t}^{xy}$ represent the active and reactive power injected by the substation at bus *i*; $P_{i,t}^{\mathrm{PV}}$ represents the PV power output at bus *i*; $L_{i,t}^{xy}$ denotes the curtailment coefficient, takes values ranging from 0 to 1, which measure the PV curtailment due to the fault.

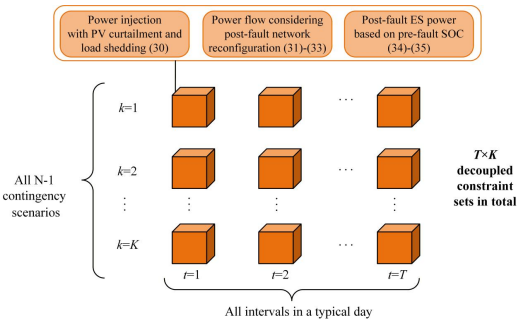

Fig. 3. Post-fault system security constraints.

B. Post-Fault Voltage and Branch Capacity Constraints

Following fault occurrence, to mitigate load shedding, the network undergoes post-fault reconfiguration. Eq. (32) represents the post-fault voltage constraints and (33) represents the post-fault branch power constraints.

$$\begin{cases} (s_{ij,t}^{xy} - 1) + r_{ij} P_{ij,t}^{xy} + x_{ij} Q_{ij,t}^{xy} \le V_{i,t}^{xy} - V_{j,t}^{xy} \\ 1 - s_{ij,t}^{xy} + r_{ij} P_{ij,t}^{xy} + x_{ij} Q_{ij,t}^{xy} \ge V_{i,t}^{xy} - V_{j,t}^{xy} \end{cases}, \quad (31)$$
$$\forall i, j \in \Omega_{\mathrm{N}},\ ij \in \Omega_{\mathrm{L}},\ t \in \Omega_{\mathrm{time}},\ xy \in \Omega_{\mathrm{F}}$$

$$V_{\min} \le V_{i,t}^{xy} \le V_{\max},\ \forall i \in \Omega_{\mathrm{N}},\ t \in \Omega_{\mathrm{time}},\ xy \in \Omega_{\mathrm{F}}, \quad (32)$$

$$\begin{cases} P_{ij,\min} \le P_{ij,t}^{xy} \le P_{ij,\max} \\ Q_{ij,\min} \le Q_{ij,t}^{xy} \le Q_{ij,\max} \end{cases}, \ \forall ij \in \Omega_{\mathrm{L}},\ t \in \Omega_{\mathrm{time}},\ xy \in \Omega_{\mathrm{F}}, (33)$$

where V_i^{xy} represents the square of the voltage at bus *i* and time *t* after the fault; P_{ij}^{xy} and Q_{ij}^{xy} represent the active and reactive power flowing through the line connecting buses *i* and *j*, respectively. $s_{ij,t}^{xy}$ denotes the switching status of branch *ij*.

C. Post-Fault ES Constraints

The same ES unit operates across both pre-fault and post-fault scenarios. During the post-fault period, its charging power must not exceed the remainder capacity, while the discharging power is constrained by the available energy capacity (subject to the pre-contingency SOC).

$$P_{\min}^{\mathrm{ess}} \le P_{i,t}^{\mathrm{ess},xy} \le P_{\max}^{\mathrm{ess}},\ \forall i \in \Omega_{\mathrm{N}},\ t \in \Omega_{\mathrm{time}},\ xy \in \Omega_{\mathrm{F}}, \quad (34)$$

$$\begin{cases} (\Gamma^{xy} - \Gamma^{xy}) P_{i,t}^{\mathrm{ess},xy} \ge (SOC - SOC_{i,t}) \\ (\Gamma_{\mathrm{RP}}^{xy} - \Gamma_{\mathrm{SW}}^{xy}) P_{i,t}^{\mathrm{ess},xy} \le (SOC_{i,t} - SOC_{\max}) \end{cases}, \quad (35)$$
$$\forall i \in \Omega_{\mathrm{N}},\ t \in \Omega_{\mathrm{time}},\ xy \in \Omega_{\mathrm{F}}$$

where $P_{i,t}^{\mathrm{ess},xy}$ denotes charging/discharging power of the ES at

bus i and time t. $\Gamma_{\mathrm{RP}}^{xy}$ denotes duration of the repair-and-switching interruptions associated with the fault of the branch connecting buses x and y. $\Gamma_{\mathrm{SW}}^{xy}$ denotes duration of the switching-only interruptions associated with the fault of the branch connecting buses x and y fault. Eq. (35) ensures that the ES system maintains sufficient capacity for charging and discharging operations during the line reconfiguration and restoration phases following a fault on line xy.

V. PV Curtailment and Reliability Constraints to Safeguard User Interests

This section elaborates on the PV curtailment constraints and reliability constraints to safeguard user interests. The McCormick envelope is employed to relax the nonlinear terms introduced by the curtailment formulation. To mitigate the approximation errors inherent in the McCormick relaxation, we propose an adaptive piecewise McCormick method.

A. Post-fault PV Curtailment Constraint

The PV curtailment constraint, corresponding to (4) in Section II, is elaborated in this section, and serves as one of the core constraints of this paper. Its content is as follows.

$$P_{i,t}^{\mathrm{curt},xy} = (1-L_{i,t}^{xy})P_{i,t}^{\mathrm{PV}},\ \forall i \in \Omega_{\mathrm{N}},\ t \in \Omega_{\mathrm{time}},\ xy \in \Omega_{\mathrm{F}}, \quad (36)$$

$$\sum_{t\in\Omega_{\mathrm{time}}}\sum_{xy\in\Omega_{\mathrm{F}}}\sum_{i\in\Omega_{\mathrm{N}}} P_{i,t}^{\mathrm{curt},xy} \le G^{\exp}, \quad (37)$$

In (30), $L_{i,t}^{xy}P_{i,t}^{\mathrm{PV}}$ denotes the energy of PV generation power integrated into the grid; $(1-L_{i,t}^{xy})P_{i,t}^{\mathrm{PV}}$ represents the curtailed PV power due to various operational constraints and system requirements. The constraints based on piecewise-McCormick are formulated as follows.

$$\begin{cases} P_{i,t}^{xy} + P_{i,t}^{\mathrm{load}}q_{i,t}^{xy} + P_{i,t}^{\mathrm{ess},xy} - Pg_{i,t}^{xy} \ge \sum_{s\in\mathrm{S}}(P_{\min}^{\mathrm{PV}}L_{i,t,s} + L_{\min,s}P_{i,t,s}^{\mathrm{PV}} - P_{\min}^{\mathrm{PV}}L_{\min,s}y_{i,t,s}) \\ P_{i,t}^{xy} + P_{i,t}^{\mathrm{load}}q_{i,t}^{xy} + P_{i,t}^{\mathrm{ess},xy} - Pg_{i,t}^{xy} \ge \sum_{s\in\mathrm{S}}(P_{\max}^{\mathrm{PV}}L_{i,t,s} + L_{\max,s}P_{i,t,s}^{\mathrm{PV}} - P_{\max}^{\mathrm{PV}}L_{\max,s}y_{i,t,s}) \\ P_{i,t}^{xy} + P_{i,t}^{\mathrm{load}}q_{i,t}^{xy} + P_{i,t}^{\mathrm{ess},xy} - Pg_{i,t}^{xy} \le \sum_{s\in\mathrm{S}}(P_{\max}^{\mathrm{PV}}L_{i,t,s} + L_{\min,s}P_{i,t,s}^{\mathrm{PV}} - P_{\max}^{\mathrm{PV}}L_{\min,s}y_{i,t,s}) \\ P_{i,t}^{xy} + P_{i,t}^{\mathrm{load}}q_{i,t}^{xy} + P_{i,t}^{\mathrm{ess},xy} - Pg_{i,t}^{xy} \le \sum_{s\in\mathrm{S}}(P_{\min}^{\mathrm{PV}}L_{i,t,s} + L_{\max,s}P_{i,t,s}^{\mathrm{PV}} - P_{\min}^{\mathrm{PV}}L_{\max,s}y_{i,t,s}) \end{cases}, \quad (38)$$

$$\forall i \in \Omega_{\mathrm{N}},\ t \in \Omega_{\mathrm{time}},\ xy \in \Omega_{\mathrm{F}}$$

$$L_{i,t} = \sum_{s\in\mathrm{S}} L_{i,t,s},\ \forall i \in \Omega_{\mathrm{N}},\ t \in \Omega_{\mathrm{time}} \quad (39)$$

$$P_{i,t}^{\mathrm{PV}} = \sum_{s\in\mathrm{S}} P_{i,t,s}^{\mathrm{PV}},\ \forall i \in \Omega_{\mathrm{N}},\ t \in \Omega_{\mathrm{time}} \quad (40)$$

$$\sum_{s\in\mathrm{S}} y_{i,t,s} = 1,\ \forall i \in \Omega_{\mathrm{N}},\ t \in \Omega_{\mathrm{time}} \quad (41)$$

$$\begin{cases} L_{\min,s} = L_{\min} + (L_{\max} - L_{\min})(s-1)/|S| \\ L_{\max,s} = L_{\max} + (L_{\max} - L_{\min})s/|S| \end{cases},\ \forall s \in \mathrm{S} \quad (42)$$

$$L_{\min,s}y_{i,t,s} \le L_{i,t,s} \le L_{\max,s}y_{i,t,s},\ \forall i \in \Omega_{\mathrm{N}},\ t \in \Omega_{\mathrm{time}},\ s \in \mathrm{S} \quad (43)$$

$$P_{\min,s}^{\mathrm{PV}}y_{i,t,s} \le P_{i,t,s}^{\mathrm{PV}} \le P_{\max,s}^{\mathrm{PV}}y_{i,t,s},\ \forall i \in \Omega_{\mathrm{N}},\ t \in \Omega_{\mathrm{time}},\ s \in \mathrm{S} \quad (44)$$

$$y_{i,t,s} \in \{0,1\},\ \forall i \in \Omega_{\mathrm{N}},\ t \in \Omega_{\mathrm{time}},\ s \in \mathrm{S} \quad (45)$$

B. Reliability Constraint

The reliability index employed in this study is quantified by the load shedding on a typical day. Based on the aforementioned model, the specific expression of (5) in Section II is presented as follows.

$$\sum_{t\in\Omega_{\mathrm{time}}}\sum_{xy\in\Omega_{\mathrm{F}}}\sum_{i\in\Omega_{\mathrm{N}}} \lambda^{xy}\Gamma_{\mathrm{SW}}^{xy}p_{i,t}^{xy}P_{i,t}^{\mathrm{load}} + \lambda^{xy}(\Gamma_{\mathrm{RP}}^{xy} - \Gamma_{\mathrm{SW}}^{xy})(1-q_{i,t}^{xy})P_{i,t}^{\mathrm{load}} \le H^{\exp} \quad (46)$$

where λ^{xy} denotes outage rate of the branch xy. $p_{i,t}^{xy}$ is a binary indicator, $p_{i,t}^{xy} = 1$ if bus i is affected by line xy failure at time t, else 0. The specific calculation methodology for these reliability indices is accomplished in [30].

C. The Trade-off Between Reliability and PV Curtailment and Its Industrial Applications

In this subsection, we identify a potential inherent trade-off between improving load-supply reliability and reducing PV curtailment under fault scenarios. That is, attempts to decrease load shedding (enhancing power supply reliability) often require greater PV curtailment. Conversely, efforts aimed at reducing PV curtailment may lead to increased load shedding (reducing power supply reliability). We guess that ES system is a key factor cause this trade-off. This relationship may further affect the effectiveness of both reliability and PV curtailment constraints, thereby posing significant challenges to the protection of interests for PV owners and load consumers. A detailed analysis of this interplay will be provided in the following case study.

Regarding the industrial application of this trade-off relationship, we will discuss it in two categories of regions: those with high power supply reliability requirements and those with low power supply reliability requirements.

For regions with high reliability demands, distributed PV integration planning should follow the intrinsic trade-off relationship. A clear PV integration and collaboration mechanism should be established. The core of this mechanism is to assess the PV owner's acceptance level for PV curtailment. If an owner seeks large-scale integration but cannot accept high post-fault PV curtailment, according to the trade-off, co-investment in additional ES with the grid operator is necessary. If the owner neither accepts significant curtailment nor is willing to co-invest in ES, the grid operator should decline the connection request. Otherwise, the owner will face unsatisfactory revenue, and the grid operator will bear additional operational risks.

If the PV owner's required integration capacity is small, making the trade-off less binding, then the aforementioned issues will not arise.

For areas with low reliability requirements (e.g., rural grids), which entails relaxing strict load shedding constraints, based on the trade-off relationship, PV curtailment can be allowed with a large adjustment room. Under such circumstances, whether PV owner require large or small integration capacities, or have high or low requirements for post-fault PV curtailment, these demands can be relatively easily accommodated.

VI. Case Studies

In this section, all case studies are implemented by CPLEX 12.1 with MATLAB 2024a on a PC with an Intel Core i5/2.7-GHz-based processor and 16 GB of RAM.

A practical 10-bus distribution system from East China, the

IEEE 33-bus test system and the 123-bus test system are used to verify the effectiveness of the proposed method and to uncover the inherent trade-off between enhancing load-supply reliability and reducing PV curtailment in the presence of ES.

A. 10-Bus Distribution Test System

The proposed approach is tested using the 10-bus distribution system [31] and presented in Fig. 4. For this system, it is considered that all the circuits have a switch. For quality requirements in this system, the lower and upper bounds of voltage magnitude are defined in 0.95 and 1.05 p. u., respectively. The system has two PV units located at buses 4 and 6, and two ES units installed at buses 3 and 7. As done in [32], all branches are equipped with a switch. The standard deviation coefficients σ^{PV} for these two PV are set to 0.05, with a correlation coefficient of 0.5. The confidence level for the chance-constrained security limitations is set to 0.95.

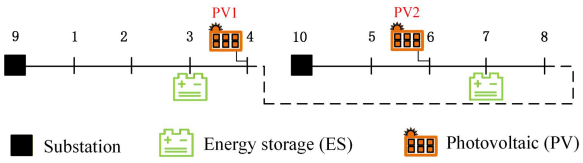

Fig. 4. Network structure of the 10-bus distribution system.

1) *Simulation Results with Basic Parameters*

Under this system, to safeguard the interests of users, we set the upper limit of PV curtailment to 4.35 MWh and the expected load shedding to 0.15 MWh. By applying the method proposed in this paper, the capacity of PV integration point 1 (PV1) is 4.2 MW, and that of PV integration point 2 (PV2) is 9.72 MW. The PVHC is 13.92 MW.

The higher integration capacity of PV2 compared to PV1 is primarily attributed to their distinct power transmission paths. The power generated by PV1 follows the transmission path: Substation 9-bus 1-bus 2-bus 3-bus 4, where each line segment is constrained by its respective thermal stability limit. When PV power is integrated at bus 4, the surplus power beyond local load consumption flows to Substation 9 through this path. In contrast, PV2 is connected at bus 7, which exhibits a shorter power transmission path. This reduced path length enables a higher capacity for reverse power flow, thereby allowing greater PV integration.

To further compare the differences between the proposed method and existing research methods, we establish three scenarios.

Scenario 1: Considering only security constraints;
Scenario 2: Incorporating post-fault PV curtailment constraints;
Scenario 3: Considering both post-fault PV curtailment and reliability constraints.

TABLE I
COMPARISON OF DIFFERENT SCENARIOS

Scenario	PVHC (MW)	Post-fault PV curtailment (MWh)	Post-fault load shedding (MWh)
Scenario 1	21.71	11.50	4.35
Scenario 2	14.17	Upper limit to 0.15	5.58
Scenario 3	13.92	Upper limit to 0.15	Upper limit to 4.35

Scenario 1 represents the result under security constraints typically considered in existing research. Comparing **Scenario 1** and **Scenario 2,** although the PVHC in **Scenario 1** is significantly higher than that in **Scenario 2**, the energy of PV curtailment in **Scenario 1** is extremely large—dozens of times greater than that in **Scenario 2**. This would severely undermine the interests of PV owners. Furthermore, the load shedding increases in **Scenario 2** compared to **Scenario 1**. This occurs because the operation of ES tends to reduce post-fault PV curtailment, thereby impairing its effectiveness in load restoration. This reflects a certain trade-off relationship between the two factors. Therefore, to simultaneously safeguard the interests of both PV owners and load consumers, both PV curtailment and load shedding can be incorporated as constraints (**Scenario 3**), which is the focus of this paper. Under these constraints, resulting in a PVHC of 13.92 MW. Compared to **Scenario 2**, the PVHC only decreases by 1.76%, while the reliability is significantly improved (load shedding is reduced by 22.04%). These results demonstrate the feasibility and effectiveness of the proposed method.

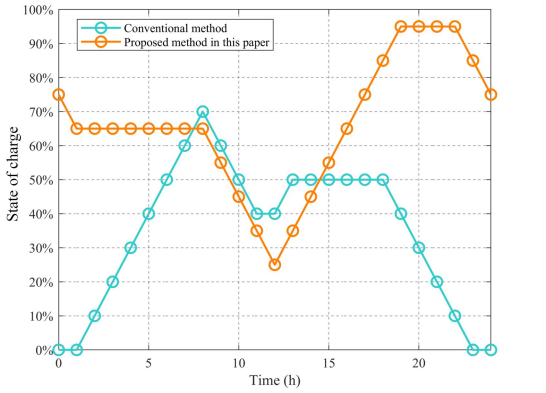

Fig. 5. Comparison of ES SOC profiles under different methods.

To investigate the behavioral differences of the ES under various methods, this study compares the SOC profiles of the ES under both the conventional method that considers only normal operating conditions and proposed method presented in this paper, which accounts for user demand both pre-fault and post-fault. The comparative results are illustrated in Fig. 5.

Under the conventional method, which does not account for post-fault PV and load loss, the SOC exhibits a wide range of variation. The ES completes a full charge–discharge cycle within a day to achieve arbitrage by leveraging the difference between peak and off-peak electricity prices. Also, The ES system is charged at 12:00 (PV output peak), with the objective of enhancing the PVHC.

The two ES SOC curves in Fig. 5 reveal significant differences in ES behavior under different methods. It can be observed that the differences between the two are manifested in two periods: 11:00-15:00 and 18:00-24:00, 00:00-10:00 (primarily nighttime). These periods reflect the effect of PV curtailment constraints and reliability constraints, respectively. The following discussion elaborates on this difference.

During the period of high PV output (11:00-15:00), the method proposed in this paper has a lower SOC level compared to the traditional method. This strategy aims to reserve sufficient capacity for post-fault charging, thereby reducing PV curtailment which demonstrates the effectiveness of the PV curtailment constraint. During the remaining periods (18:00-24:00, 00:00-10:00), the proposed method maintains a higher SOC than the traditional method. This is to ensure that the ES retains sufficient energy to support the load after the

fault, thereby reducing load shedding.

Additionally, for the proposed method, the ES charge during periods of high PV output in the pre-fault to enhance the system's PVHC, while also achieving arbitrage through intraday charging and discharging cycles. Under post-fault, considerations for load support require reserving storage capacity during daytime and increasing charging at night, which puts the pre-fault operational trend and post-fault requirements in conflict. Since reliability constraints and PV curtailment constraints are both hard limits, whereas maximizing PVHC and achieving arbitrage are optimization objectives, the resulting SOC curve of the ES essentially reflects an effort to optimize pre-fault operational goals (namely, PVHC and arbitrage) as much as possible while satisfying the two post-fault constraints.

To further validate the effectiveness of the proposed method, a comparative analysis is conducted. with an evaluation approach based on a fixed curtailment ratio cap, assuming no reliability constraints in this comparison.

Maintaining the same total curtailed PV energy, the comparison is designed as follows: First, the PVHC of the system is evaluated based on a fixed curtailment cap, and the corresponding total curtailed PV energy is calculated. Subsequently, this curtailed energy is incorporated as a constraint into the proposed evaluation framework to recalculate the PVHC. The comparison results of these two methods are presented in Table II.

TABLE II
COMPARISON OF DIFFERENT CURTAILMENT CONSTRAINT METHODS

Curtailment ratio	Curtailment energy	Set fixed curtailment ratio cap method [14]		Proposed method	
		PVHC	PV generation output	PVHC	PV generation output
7%	0.61 MWh	15.19 MW	109.52 MWh	17.61 MW	127.06 MWh
10%	0.89 MWh	15.37 MW	110.54 MWh	18.52 MW	133.38 MWh

The results above indicate that the proposed method yields a higher PVHC compared to the approach with a fixed curtailment ratio cap. This is because the fixed curtailment method imposes a uniform curtailment constraint on all PV integration points, failing to fully account for differences in NT and the actual operational requirements at different buses. As a result, the method of [14] lacks flexibility. In contrast, the proposed method enables differentiated PV curtailment strategy based on the actual operational conditions of each PV location. Under the same total curtailment amount, the proposed method offers greater flexibility and adaptability, thereby supporting higher PV integration capacity and achieving greater PV power generation.

2) *Adaptive McCormick Envelope Verification*

The piecewise McCormick envelope can more effectively reduce errors. Increasing the number of partitions strengthens the relaxation at the cost of higher computational effort to solve the resulting mixed-integer problem. Empirically, the algorithm performs well with four partitions. Simulation analysis reveals that the curtailment coefficient $L_{i,t,s}$ exhibits high-density distribution (85% of observations) within [0.8,1]. Consequently, the original uniform quadripartition (0.25 interval width) is adapted to a non-uniform partitioning. This scheme compresses the local envelope width in the high-density region. As validated experimentally, the adaptive McCormick envelope significantly reduces relaxation errors for the bilinear term $P_{i,t}^{\mathrm{PV}} L_{i,t}^{xy}$ by 49.37%.

3) *Sensitivity Analysis*

(a) *PV Curtailment*

By setting the expected load shedding to 4.35 MWh, the PVHC is evaluated under varied PV curtailment levels, as demonstrated in Fig. 6.

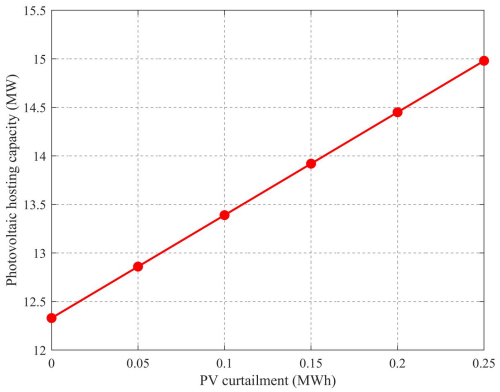

Fig. 6. Curve of PVHC variation with PV curtailment.

In Fig. 6, when set the expected load shedding at 4.35 MWh as the PV curtailment constraints increase from 0 to 0.25MWh, the PVHC increase from 12.33 MW to 14.98MW. As the allowable PV curtailment rate increases, the system's PVHC correspondingly rises. This occurs because when PV installed capacity approaches the system's operational limits, power injection elevates bus voltages to the allowable upper limit. By proactively curtailing the energy of PV generation that would otherwise cause voltage violations, the system can safely accommodate additional PV installed capacity.

(b) *Load Shedding*

By setting the upper limit of PV curtailment to 0.1MWh, the PVHC is tested with varied load shedding, shown in Fig. 7.

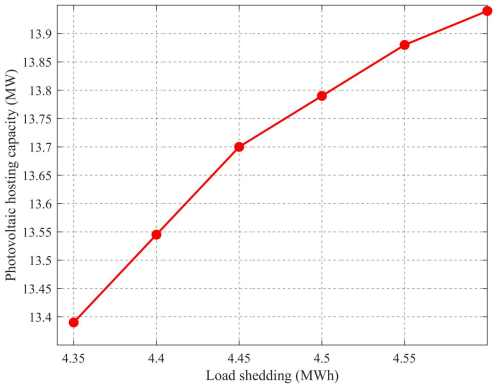

Fig. 7. Curve of PVHC variation with load shedding.

In Fig. 7, when the upper limit of PV curtailment is maintained 0.1MWh, as the load shedding constraints increase from 4.35 to 4.6MWh, the PVHC increase from 13.39 MW to 13.94 MW. This increase in PVHC can be attributed to the relaxed load-shedding constraint, which reduces the requirement for ES systems to provide supportive discharge during post-fault restoration. Consequently, a greater portion of the storage capacity can be allocated to mitigating voltage

violations and power flow limits, thereby unlocking further potential for PVHC.

4) *Uncertainty Parameters Analysis*

For regions without existing PV integration, when evaluating PVHC, coefficients can initially be assumed. After PV systems have been preliminarily integrated, if an assessment of the additional PV capacity that can be integrated is required, the continuously collected actual PV output data can be used to dynamically calibrate the initial coefficients through statistical methods [38]. This iterative process enables the uncertainty characterization in the model to gradually align with the actual operational characteristics of the system, thereby enhancing the accuracy and reliability of the evaluation results.

(a) *Standard Deviation Coefficients*

The impact of power fluctuations is further discussed in this section. The standard deviation coefficients vary from 0.05 to 0.1. PVHC becomes smaller along with the enlargement of standard deviations.

TABLE III
COMPARISON OF DIFFERENT STANDARD DEVIATION COEFFICIENTS

Standard deviation coefficients	0.05	0.075	0.1
PVHC	13.92MW	12.60MW	11.29MW

(b) *Correlation Coefficients*

To test the impact of correlations in uncertainties, the correlation coefficients of random variables vary from 0.3 to 0.7. PVHC becomes smaller along with the increase of correlation coefficients

TABLE IV
COMPARISON OF DIFFERENT CORRELATION COEFFICIENTS

Correlation coefficients	0.3	0.5	0.7
PVHC	14.83MW	13.92MW	13.01MW

5) *Trade-off Relationship Between PV Curtailment and Load Shedding*

In Section V, we briefly introduced the trade-off relationship between PV curtailment and load shedding. In this section we analyze this relationship in detail through three case studies and present the corresponding results in Table V.

***Case 1*:** Basic parameters;

***Case 2*:** Tighten the upper limit constraint on PV curtailment;

***Case 3*:** Adjust the expected load shedding to restore the PVHC in ***Case 1*.**

TABLE V
THE TRADE-OFF BETWEEN PV CURTAILMENT AND LOAD SHEDDING

Case	Load shedding (MWh)	PV curtailment (MWh)	PVHC (MW)
Case 1	4.35	0.15	13.92
Case 2	4.35	0.1	13.39
Case 3	4.57	0.1	13.92

As illustrated in the Table IV, under the basic parameters (**Case 1**), the PV curtailment is 4.35MWh, load shedding is 0.1MWh, and the PVHC reaches 13.92MW. When permitted PV curtailment limit is reduced from 0.15MW to 0.1MW to safeguard the interests of PV owners, the PVHC decreases to 13.39MW (**Case 2**). Maintaining the original PVHC level requires increasing the upper limit of expected load shedding (**Case 3**), which may adversely affect the interests of users. ES plays a critical role in this trade-off relationship. To further reduce load shedding, it is necessary to either enhance the discharge capability of ES or accept greater PV curtailment (and vice versa). This is duo to the fact that when reducing load shedding, the ES system must discharge to support the grid. However, owing to the inherent operational constraint that storage systems cannot charge and discharge simultaneously, once operating in discharge mode, they cannot store excess PV energy through charging. Therefore, to balance the interests of both PV owners and load users, appropriate values of PV curtailment and load shedding constraints must be carefully determined.

B. *IEEE 33-Bus Test System*

In Fig. 8, the IEEE 33-bus system is used to verify the effectiveness of the proposed methods This system has been widely used [34]. It is considered that all the circuits have a switch. For quality requirements in this system, the lower and upper bounds of voltage magnitude are defined in 0.95 and 1.05 p.u., respectively. The system has three PV units localized at buses 14, 21, and two ES units installed at buses 9 and 20.

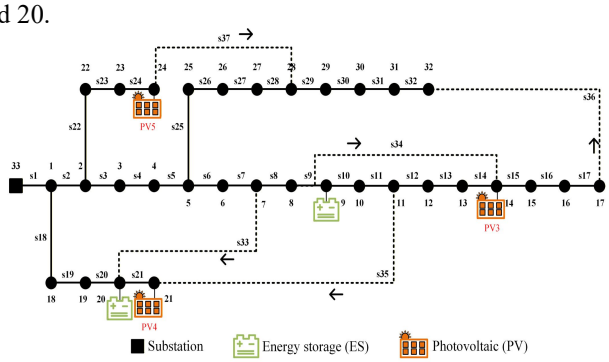

Fig. 8. Network structure of the IEEE 33-bus test system.

The total load of this system is 67 MW; therefore, we set the upper limit of PV curtailment to 0.1 MWh and the expected load shedding to 2.22 MWh. The specific results are presented in Table VI.

TABLE VI
EVALUATION RESULTS OF IEEE 33-BUS SYSTEM

PV3	PV4	PV5	PVHC
0.86MW	1.59MW	1.84MW	4.29MW

For the distribution system with 33 buses and 37 branches, considering fault scenarios on 31 lines and the availability of 5 tie switches for post-fault network reconfiguration, the formulated model involves approximately 24,000 variables, including 3,840 integer variables. At this scale, the solution time is approximately 5 minutes.

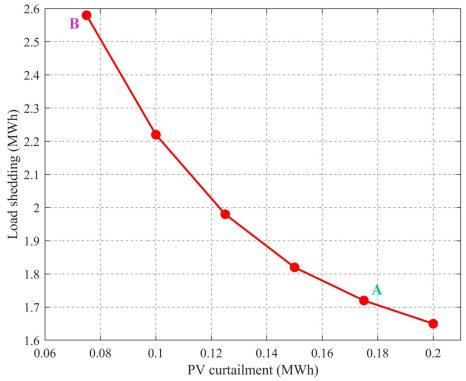

Fig. 9. Trade-off curve between PV curtailment and load shedding.

Fig. 9 depicts the variation of PV curtailment and load shedding for a PVHC maintained at 4.29 MW. The upper limit of PV curtailment and the expected load shedding were adjusted to maintain a constant PVHC, resulting in the presented curve. This curve visually illustrates the trade-off relationship between PV curtailment and load shedding. Based on the points A and B on the curve, we present and analyze the ES behavior at points A and B in Fig. 10.

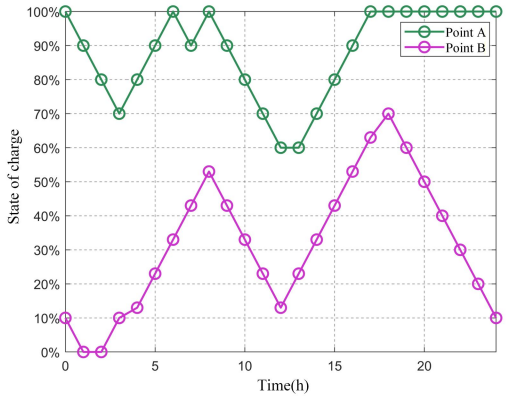

Fig. 10. ES profile of Point A and Point B.

At Point A, where the operational strategy of the ES system prioritizes ensuring load restoration, its SOC curve generally remains at a higher level, since the ES must maintain sufficient available energy to support post-fault load supply. However, maintaining a consistently high SOC level means the available charging room becomes correspondingly limited, thereby compromising its ability to suppress post-fault PV curtailment.

At Point B, where ES system prioritizes limiting PV curtailment, its capability for load restoration is correspondingly weakened. As observed from the ES SOC curve, the overall level remains in a lower range, primarily to reserve sufficient charging room for reducing post-fault PV curtailment. However, this strategy also limits the available discharging room of the ES during periods without PV output, thereby undermining its support capability for post-fault load restoration.

C. IEEE 123-Bus Test System

To validate the scalability of the proposed method, we use the IEEE 123-bus distribution system, which operates at a nominal voltage of 4.16 kV. The structure is presented in Fig. 11. The system has four distributed PV (PV8, PV9, PV10 and PV11) and three ES units installed at buses76, 95, and 300.

We set the upper limit of PV curtailment to 0.1 MWh and the expected load shedding to 1.96 MWh to validate the effectiveness of the method. The specific results are presented in Table VII which demonstrates the scalability of the method proposed in this paper.

For a distribution network system with 123 buses and 122 branches, considering fault scenarios involving 117 lines and the participation of 5 tie switches in post-fault network reconfiguration, the model involves approximately 250,000 variables, including 4,200 integer variables. At this scale, the solution time is approximately 70 minutes, which is about 14 times that required for the 33-bus system. The increase in solution time exhibits a moderate growth with the system scale and the number of fault scenarios. Since the PVHC assessment problem does not impose stringent requirements on solution time, the computational time for the 123-bus system remains within an acceptable range. This demonstrates that the proposed method maintains good computational efficiency and scalability even when dealing with complex systems.

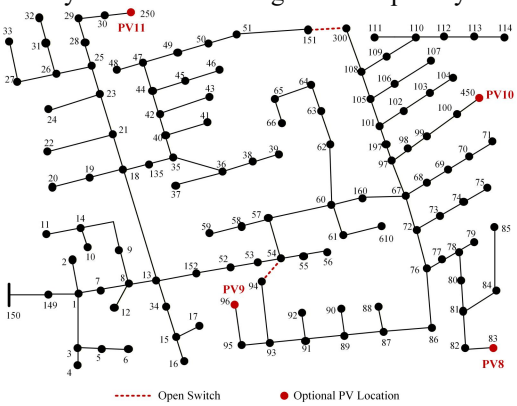

Fig.11. Network structure of the IEEE 123-bus test system.

TABLE VII
EVALUATION RESULTS OF IEEE 123-BUS SYSTEM

PV8	PV9	PV10	PV11	PVHC
2.22MW	2.49MW	2.06MW	2.38MW	9.15MW

VII. CONCLUSION

In this work, a PVHC assessment method for distribution networks is proposed, which considers post-fault PV curtailment and load shedding constraints. The method ensures secure grid operation while safeguarding the interests of PV owners and load consumers. The main conclusions of this study are as follows.

(a) The proposed bi-scenario PVHC assessment method embeds PV curtailment constraints and reliability constraints to safeguard the interests of PV owners and load consumers. We uncover the inherent trade-off between enhancing load-supply reliability and reducing fault-induced PV curtailment by incorporating ES.

(b) The case study verifies the effectiveness of the proposed post-fault interests safeguarding constraints by comparing the ES SOC under the conventional method with that of the method proposed method. The sensitivity analysis indicates that tightening the upper limits of both the PV curtailment and reliability constraints decreases the PVHC. Increasing the standard deviation coefficients and correlation coefficients will lead to a more conservative PVHC. The case study of IEEE 33-bus test system and IEEE 123-bus test system indicates the acceptable computational feasibility and scalability of the method.

In the future, we will focus on integrating diverse flexible resources such as adjustable loads and electric vehicles to establish a multi-resource coordinated PVHC assessment framework with the proposed post-analysis, thereby enhancing the system's adaptability to high-penetration PV integration.

REFERENCES

[1] Diab, N. Damianakis, G. R. Chandra-Mouli, and P. Bauer, “A shared PV system for transportation and residential loads to reduce curtailment and the need for storage systems,” *Appl. Energy*, vol. 353, pp. 122131, no. 122131, Jan. 2024.

[2] S. Hashemi, J. Østergaard, T. Degner, R. Brandl, and W. Heckmann, "Efficient control of active transformers for increasing the PV hosting capacity of LV grids," IEEE Trans. Ind. Inform., vol. 13, no. 1, pp. 270-281, Feb. 2017.

[3] R. Saeedi, S. K. Sadanandan, A. K. Srivastava, K. L. Davies, and A. H. Gebremedhin, "An adaptive machine learning framework for behind the-meter load/PV disaggregation," *IEEE Trans. Ind. Inform*., vol. 17, no. 10, pp. 7060-7069, Oct. 2021.

[4] X. Chen, Z. Zhang, A. Qiu, Z. Xia, and N. N. Xiong, "Novel coverless steganography method based on image selection and StarGAN," IEEE Trans. Netw. Sci. Eng., vol. 9, no. 1, pp. 219-230, Jan./Feb. 2022.

[5] E. Mulenga, M. H. Bollen, and N. Etherden, "A review of hosting capacity quantification methods for photovoltaics in low-voltage distribution grids," *Int. J. Electr. Power Energy Syst*., vol. 115, pp. 105445, Feb. 2020.

[6] E. Kazemi-Robati, M. S. Sepasian, H. Hafezi, and H. Arasteh, "PV hosting-capacity enhancement and power-quality improvement through multi-objective reconfiguration of harmonic-polluted distribution systems," *Int. J. Electr. Power Energy Syst*., vol. 140, pp. 107972, Feb. 2022.

[7] H. Yao, W. Qin, X. Jing, Z. Zhu, K. Wang et al, "Possibilistic evaluation of photovoltaic hosting capacity on distribution networks under uncertain environment," *Appl. Energy*, vol. 324, pp. 119681, Oct. 2022.

[8] E. Mulenga and N. Etherden, "Multiple distribution networks hosting capacity assessment using a stochastic approach," *Sustainable Energy Grids Netw.*, vol. 36, pp. 101170, Dec. 2023.

[9] D. Chathurangi, U. Jayatunga, S. Perera, A. P. Agalgaonkar, and T. Siyambalapitiya, "A nomographic tool to assess solar PV hosting capacity constrained by voltage rise in low-voltage distribution networks," *Int. J. Electr. Power Energy Syst.*, vol. 134, pp. 107409, Jan. 2022.

[10] S. Zhang, S. Ge, H. Liu et al, "Model and observation of the feasible region for PV integration capacity considering Wasserstein-distance based distributionally robust chance constraints," *Appl. Energy*, vol. 347, pp. 121312, Oct. 2023.

[11] J. M. Home-Ortiz, O. D. Melgar-Dominguez, M. S. Javadi, J. R. S. Mantovani, and J. P. S. Catalão, "Improvement of the distribution systems resilience via operational resources and demand response," *IEEE Trans. Ind. Appl.*, vol. 58, no. 5, pp. 5966-5976, Sep. 2022.

[12] Q. Chai, C. Zhang, Z. Tong, S. Lu, W. Chen, and Z. Y. Dong, "PV inverter reliability constrained volt/Var control with power smoothing via a convex–concave programming method," *IEEE Trans. Ind. Inform*., vol. 19, no. 1, pp. 109–120, Jan. 2023.

[13] Q. Gu, Q. Y. Chang, N. Xiong, and L. Chen, "Forecasting Nickel futures price based on the empirical wavelet transform and gradient boosting decision trees," Appl. Soft Comput., vol. 109, p. 107472, Sep. 2021.

[14] J. M. Home-Ortiz, O. D. Melgar-Dominguez, J. R. S. Mantovani, and J. P. S. Catalão, "PV hosting capacity assessment in distribution systems considering resilience enhancement," *Sustain. Energy, Grids Netw*., vol. 32, pp.100829, Dec. 2022.

[15] M. Alanazi, A. Alanazi, M. A. Akbari, M. Deriche, and Z. A. Memon, "A non-simulation-based linear model for analytical reliability evaluation of radial distribution systems considering renewable DGs," Appl. Energy, vol. 342, pp. 121153, Jul. 2023.

[16] Z. Li, W. Wu, X. Tai, and B. Zhang, "A reliability-constrained expansion planning model for mesh distribution networks," *IEEE Trans. Power Syst.*, vol. 36, no. 2, pp. 948-960, Mar.2021.

[17] X Shen, B Yi, H Liu, W Zhang, Z Zhang, S Liu, N Xiong, "Deep variational matrix factorization with knowledge embedding for recommendation system," *IEEE Trans. Knowl. Data Eng* , vol. 33, no. 5, pp. 1906–1918, May 2021.

[18] G. Muñoz-Delgado, J. Contreras, and J. M. Arroyo, "Reliability assessment for distribution optimization models: A non-simulation-based linear programming approach," *IEEE Trans. Smart Grid*, vol. 9, no. 4, pp. 3048-3059, Jul. 2018.

[19] X. Lu, X. Fan, H. Qiu, W. Gan, S. Xia et al, "Machine learning based uncertainty-alleviating operation model for distribution systems with energy storage," *Journal of Modern Power Systems and Clean Energy*, vol. 12, pp. 1605-1616, Sep. 2024.

[20] Y. Chen, Y. Liu, H. Yin, Z. Tang, G. Qiu, and J. Liu, "Multiagent soft actor–critic learning for distributed ESS enabled robust voltage regulation of active distribution grids," *IEEE Trans. Ind. Inform*., vol. 20, no. 9, pp. 11069-11080, Sep. 2024.

[21] R. Peesapati, V. K. Yadav, K. Singh, and S. Ghosh, "Optimal scheduling of bess for congestion management considering reliability and OTS," *Sustain. Energy, Grids Netw*., vol. 38, pp. 101227, Jun. 2024.

[22] N. Xiong, A. V. Vasilakos, L. T. Yang, L. Song, and Y. Pan, "A novel self-tuning feedback controller for active queue management supporting TCP flows," Inf. Sci., vol. 180, no. 11, pp. 2249–2263, Jun. 2010.

[23] S. Lee, D. H. Choi, "Learning and unlearning to operate profitable secure electric vehicle charging," *IEEE Trans. Ind. Inform*., vol. 20, no. 9, pp. 11213-11223, Sep. 2024.

[24] D. Zhang, G. M. Shafiullah, C. K. Das, and K. W. Wong, "Optimal allocation of battery energy storage systems to improve system reliability and voltage and frequency stability in weak grids," *Appl. Energy*, vol. 377, pp. 124541, Jan. 2025.

[25] R. Zafar and H. R. Pota, "Multi-timescale coordinated control with optimal network reconfiguration using battery storage system in smart distribution grids," *IEEE Trans. Sustain. Energy.*, vol. 14, no. 4, pp. 2338-2350, Oct. 2023.

[26] Y. Chen, Y. Liu, H. Yin, Z. Tang, G. Qiu, and J. Liu, "Multiagent soft actor–critic learning for distributed ESS enabled robust voltage regulation of active distribution grids," *IEEE Trans. Ind. Inform*., vol. 20, no. 9, pp. 11069-11080, Sep. 2024.

[27] Q. Fu, C. Dai, S. Bu et al, "Integrating power electronics-based energy storages to power systems: A review on dynamic modeling, analysis, and future challenges," *Renewable and Sustainable Energy Reviews*, vol. 213, p. 115460, May 2025.

[28] S. Zhang, S. Ge, H. Liu et al, "Region-based flexibility quantification in distribution systems: an analytical approach considering spatio-temporal coupling," *Appl. Energy,* vol. 355, p. 122175, Feb. 2024.

[29] S. Zhang, S. Ge, H. Liu et al, "Distributionally robust hierarchical multi-objective voltage risk management for unbalanced distribution systems," *Int. J. Electr. Power Energy Syst*, vol. 154, pp. 109446, Dec. 2023.

[30] Z. Li, W. Wu, B. Zhang, and X. Tai, "Analytical reliability assessment method for complex distribution networks considering post-fault network reconfiguration," *IEEE Trans. Power Syst*., vol. 35, no. 2, pp. 1457-1467, Mar. 2020.

[31] C. Zhu et al., "Feasibility analysis of PV and energy storage system integration for flexible distribution networks: A moment-based distributionally robust approach," *Energy Rep*., vol. 9, pp. 89-98, May 2023.

[32] A. Tabares, G. Munoz-Delgado, J. F. Franco, J. M. Arroyo, and J. Contreras, "An enhanced algebraic approach for the analytical reliability assessment of distribution systems," *IEEE Trans. Power Syst*, vol. 34, no. 4, pp. 2870-2879, Jul. 2019.

[33] J. Wang, Q. Wang, X. Xing, Z. Fu, C. Hai, and H. Liu, "Feasible region analysis of PV hosting capacity in active distribution networks via a two-stage optimization approach," *Electr. Power Syst. Res.*, vol. 242, p. 111446, May 2025.

[34] J. Guo, A. Liu, K. Ota, M. Dong, X. Deng, and N. N. Xiong, "ITCN: An intelligent trust collaboration network system in IoT," *IEEE Trans. Netw. Sci. Eng.*, vol. 9, no. 1, pp. 203-218, Jan./Feb. 2022.

[35] R. K. Gupta, D. K. Molzahn, "Improving fairness in photovoltaic curtailment via feedback-driven daily topology reconfiguration in power distribution networks," *Appl. Energy*, vol.400, pp. 126543, Dec. 2025.

[36] X. Ran, W. P. Tay, and C. Lee, "High-performance optimization model based on novel conditional value at risk metric for power grids with high wind power penetration," *IEEE Trans. Ind. Inform*., vol. 21, no. 7, pp. 5689-5700, Jul. 2025.

[37] F. Bouffard and F. D. Galiana, "Stochastic security for operations planning with significant wind power generation," *IEEE Trans. Sustain. Energy*, vol. 23, no. 2, pp. 306–316, May 2008.

[38] G. R. Shorack, *Probability for Statisticians*. New York, NY, USA: Springer, 2000.